

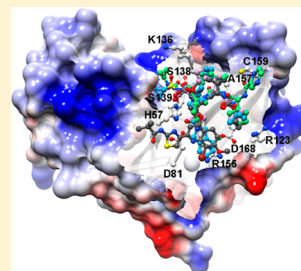
Key Binding and Susceptibility of NS3/4A Serine Protease Inhibitors against Hepatitis C Virus

Arthitaya Meeprasert,[†] Supot Hannongbua,[†] and Thanyada Rungrotmongkol^{*,‡}

[†]Computational Chemistry Unit Cell, Department of Chemistry, Faculty of Science, Chulalongkorn University, 254 Phayathai Road, Pathumwan, Bangkok 10330, Thailand

[‡]Department of Biochemistry, Faculty of Science, Chulalongkorn University, 254 Phayathai Road, Pathumwan, Bangkok 10330, Thailand

ABSTRACT: Hepatitis C virus (HCV) causes an infectious disease that manifests itself as liver inflammation, cirrhosis, and can lead to the development of liver cancer. Its NS3/4A serine protease is a potent target for drug design and development since it is responsible for cleavage of the scissile peptide bonds in the polyprotein important for the HCV life cycle. Herein, the ligand-target interactions and the binding free energy of the four current NS3/4A inhibitors (boceprevir, telaprevir, danoprevir, and BI201335) were investigated by all-atom molecular dynamics simulations with three different initial atomic velocities. The per-residue free energy decomposition suggests that the key residues involved in inhibitor binding were residues 41–43, 57, 81, 136–139, 155–159, and 168 in the NS3 domain. The van der Waals interactions yielded the main driving force for inhibitor binding at the protease active site for the cleavage reaction. In addition, the highest number of hydrogen bonds was formed at the reactive P1 site of the four studied inhibitors. Although the hydrogen bond patterns of these inhibitors were different, their P3 site was most likely to be recognized by the A157 backbone. Both molecular mechanic (MM)/Poisson–Boltzmann surface area and MM/generalized Born surface area approaches predicted the relative binding affinities of the four inhibitors in a somewhat similar trend to their experimentally derived biological activities.



INTRODUCTION

Over 170 million people worldwide are infected with hepatitis C virus (HCV), and this is increasing at about 3–4 million people every year.¹ Importantly, HCV is one of the major causes of liver inflammation which can eventually lead to cirrhosis and in some cases might develop to hepatocellular carcinoma or liver cancer.^{1,2} Regrettably, the approved anti-HCV drugs (ribavirin, peg-interferon, boceprevir, and telaprevir) require a long duration of treatment with a very high cost as well as inducing some side effects, such as flu-like symptoms, anemia, and hemolysis in HCV patients.^{3,4} Treatment with ribavirin in combination with peg-interferon (PEG-IFN) shows only about a 40–50% success rate of HCV genotype 1 treatment.^{5,6} This combination is used for inhibiting the polymerase and/or inosine monophosphate dehydrogenase, whereas the α -ketoamide inhibitors, boceprevir and telaprevir, target the NS3/4A protease. Consequently, the potentially promising high potent and selective noncovalent inhibitors, danoprevir (ITMN-191) and BI201335, were designed against the HCV protease. These two inhibitors are currently in phase 2 and phase 3 clinical trials, respectively.⁷ In preclinical profiles, danoprevir presented a very high inhibition of all six HCV genotypes,⁸ while BI201335 displayed a high level of efficacy in inhibiting HCV protease genotypes 1 and 4–6 but was dramatically less effective against the other genotypes.⁹ The NS3/4A protease in the complex with each of the four aligned inhibitors is shown in Figure 1. Up to date, a comparative understanding of drug-target interactions of the α -ketoamide and noncovalent inhibitors binding to the NS3/4A protease of HCV has not been provided yet. In this study

conventional molecular dynamics (MD) simulations were performed to achieve this goal.

HCV is a positive-sense single-stranded (ss)RNA virus in the *Hepacivirus* genus (*Flaviviridae* family) encoding for approximately 3000 amino acids. After ssRNA translation, the polyprotein encodes for four structural proteins (C, E1, E2, and p7), and six nonstructural proteins (NS2, NS3, NS4A, NS4B, NSSA, and NSSB) are subsequently produced by cleavage by protease enzymes of host cell and HCV origin. Among the nonstructural proteins, the NS3 serine protease complexed with the NS4A cofactor and NSSB polymerase play an essential role in the viral replication process and so become one of the most attractive targets for anti-HCV drug design and development.^{10–13} The NS3/4A cleaves the scissile peptide bond between the nonstructural proteins, NS3/NS4A (self-cleavage), NS4A/NS4B, NS4B/NSSA, and NSSA/NSSB, recognizing the D/EXXXXC/T-S/A amino acid sequence.^{14,15} The 180 amino acids at the N-terminus of the NS3 protein and 14 amino acids of the NS4A cofactor have been shown to be essential for NS3/4A activity.^{1,14,16} Without the NS4A cofactor, the HCV protease activity and cleavage rate acceleration are dramatically reduced due to the conformational change of the catalytic residues in the NS3 active site.^{14,17}

Based on the reported crystal structures of the HCV NS3/4A protease,^{18–21} the active site located on a solvent exposable surface has a rather shallow pocket (Figure 1A) in comparison with the other chymotrypsin-like proteases.^{22–24} This leads to a

Received: October 22, 2013

Published: March 14, 2014



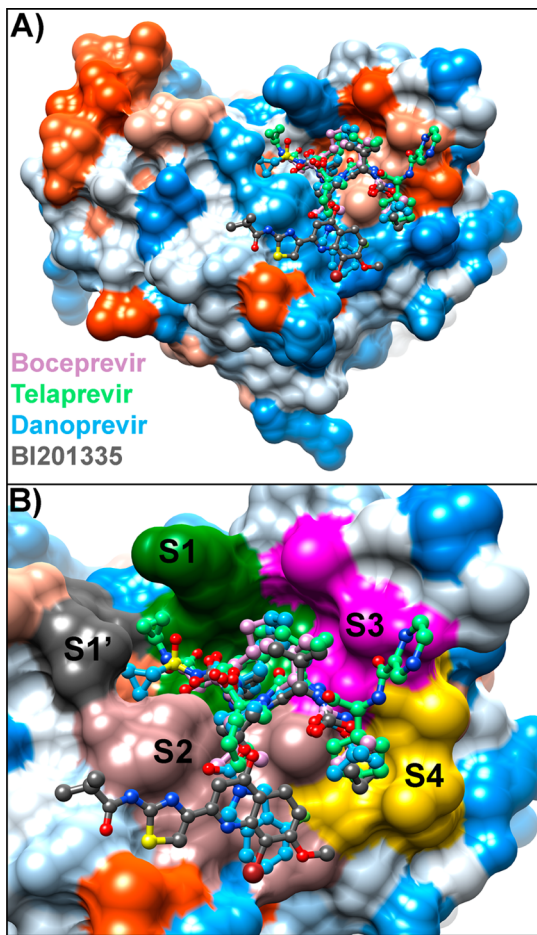


Figure 1. (A) The four current inhibitors (boceprevir, telaprevir, danoprevir, and BI201335 shown by ball and stick model) binding to the active site of the HCV protease where the most hydrophilic and hydrophobic surface shaded by blue and orange red, respectively. (B) Close view of inhibitors at the S1'-S4 site areas divided from the active site of the HCV protease.

more challenging drug design and development. The designed protease inhibitors have generally been modified from the decapeptide (P6–P4') substrate and its cleaved products.^{25–28} For example, the scissile peptide bond has been substituted with α -ketoamide for boceprevir and telaprevir, sulfonate for danoprevir, or carboxylate for BI201335 (Figure 2).

In this work, the all atomistic MD simulations in conjunction with binding free energy calculations were applied on the HCV NS3/4A protease in complex with its four inhibitors (boceprevir, telaprevir, danoprevir, and BI201335) in order to investigate the key binding pattern, drug-target interactions, and drug susceptibility. The theoretical information on drug specificity and targeted inhibition should be useful for HCV antiviral drug design and development.

MATERIALS AND METHODS

Starting Models and System Preparation. The structure of the NS3/4A protease of HCV genotype 1a with boceprevir, tetrapeptide inhibitor (similar to telaprevir), danoprevir (ITMN-191), and BI201335 (the last one is found in genotype 1b) bound were obtained from the respective crystal structures (Protein Data Bank (PDB) entry codes 2OC8,²⁰ 2PS9,¹⁹ 3MSL,²¹ and 3P8N¹⁸) and were then separately prepared as follows. To build the NS3/4A-telaprevir complex, the P4 moiety of the

tetrapeptide inhibitor was only modified to the cyclohexyl-2-pyrazin-2-ylcarbonyl of telaprevir. From the crystallization process, the catalytic S139 residue in the danoprevir complex was mutated to alanine using the site-directed mutagenesis,²¹ and so in this study the A139 residue was changed back to S139. The cocrystal structure of BI201335 bound to NS3/4A is of the HCV genotype 1b, and so the relevant 20 different amino acid residues were modeled to be the same residues as found in HCV genotype 1a from the H77 strain as well as amino acid sequence of the PDB entry code 2OC8²⁰ using the protein preparation tool implemented in Discovery Studio 2.5^{Accelrys Inc.}

All system preparations and MD simulation processes were performed on the AMBER10 package program.²⁹ The protonation states of the ionizable amino acids, lysine (K), arginine (R), histidine (H), aspartic acid (D), and glutamic acid (E), were characterized by PROPKA 3.1.³⁰ Note that the two catalytic residues H57 and D81 were ionized as the neutral histidine with protonated δ -NH (HID type) and negatively charged aspartate in the boceprevir, telaprevir, and danoprevir systems. For the BI201335 complex, the protonated ϵ -NH (HIE type) H57 and neutral aspartic acid D81 were used as derived from the ^1H NMR data.¹⁸ The missing hydrogen atoms were added using the LeaP module in AMBER10. The AMBER ff03 force field was applied for the protein.³¹ To prepare the partial atomic charges and parameters of each inhibitor, the structure was fully optimized by means of the HF/6-31g(d) level of theory using Gaussian03.³² The electrostatic potential (ESP) charges were consequently computed with the same method and basis set. The antechamber package was employed to convert ESP charges to restrained ESP (RESP) charges. The AMBER ff03 force field³¹ and general AMBER force field (GAFF)³³ were adopted for ligand parameters by the parmchk program.

In order to find the optimum structures of the NS3/4A complex, the hydrogen atoms were minimized with 1500 steps of steepest descents (SD) and followed by 1500 steps of conjugated gradient (CG) using the SANDER module implemented in AMBER10 to diminish the bad contacts and steric hindrances. Each system was subsequently solvated with the TIP3P water model³⁴ in a cubic box within 10 Å around the protein surface, and chloride counterions were added to neutralize the total positive charge of the complex. Afterward, the SD and CG minimizations with 1500 steps were respectively applied to optimize the counterions and water molecules, whereas the proteins and inhibitor were constrained with a force constant of 500 kcal/mol·Å². Finally, the whole complex was kept free of any constraint and eventually minimized with 1500 steps each for SD and CG.

Molecular Dynamics (MD) Simulations. Each prepared NS3/4A-inhibitor complex was performed by three independent MD simulations with different initial atomic velocities (namely MD1-MD3) under a periodic boundary condition with the *NPT* ensemble. All covalent bonds involving hydrogen atoms in each system were constrained with the SHAKE algorithm.³⁵ The short-range cutoff of 10 Å for nonbonded interactions was applied, while the particle mesh Ewald (PME) summation method³⁶ was used for calculating the long-range electrostatic interactions. The simulation time step was of 0.2 ps. The system was initially heated up to 298 K for 200 ps and was then simulated at this temperature at 1 atm till 40 ns. The trajectories were collected every 2 ps for analysis. The root-mean square displacement (RMSD) and hydrogen bond (H-bond) were explored using the ptraj module of AMBER, while the per-residue decomposition of MM/GBSA binding

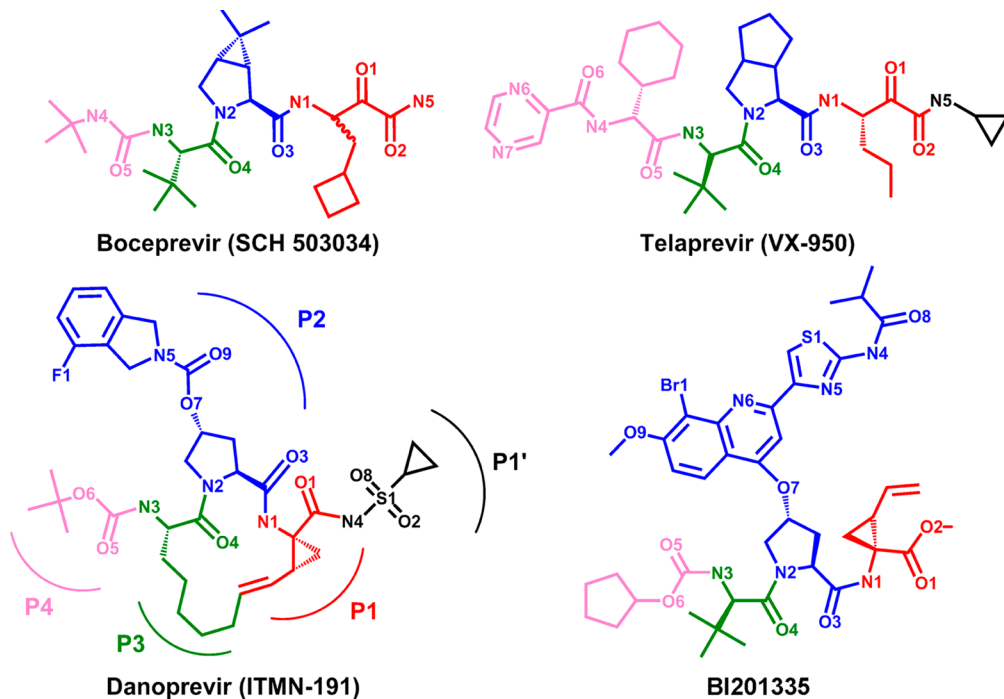


Figure 2. Chemical structures of the four NS3/4A protease inhibitors boceprevir (SCH 503034), telaprevir (VX-950), danoprevir (ITMN-191), and BI201335. The P1', P1, P2, P3, and P4 substituents are colored by black, red, blue, green, and purple, respectively.

free energy ($\Delta G_{bind}^{residue}$) and the total binding free energy (ΔG_{bind}) were calculated by means of MM/PBSA and MM/GBSA approaches using the mm_pbsa module.

Binding Free Energy. The MM/PBSA and MM/GBSA approaches have been widely succeeded in predicting the binding free energies (ΔG_{bind}) of many biomolecular systems.^{37–42} In this study, both methods were applied to estimate the (ΔG_{bind}) between the NS3/4A protease and each ligand by computing $\Delta\Delta G_{bind}$ as the free energy difference between the complex (ΔG_{com}), protein (ΔG_{prot}), and ligand (ΔG_{lig}) as shown in eq 1.

$$\Delta\Delta G_{bind} = \Delta G_{com} - (\Delta G_{prot} + \Delta G_{lig}) \quad (1)$$

Each term was achieved from the averaged free energy over 100 trajectories taken from the last 20-ns simulation. The free energy was calculated separately from the enthalpy in the gas phase (ΔH) and the entropy term ($-T\Delta S$), as shown in eq 2.

$$\Delta G = \Delta H - T\Delta S \approx \Delta E_{MM} + \Delta G_{solv} - T\Delta S \quad (2)$$

The ΔH of the system was predicted from the summation of the gas phase (ΔE_{MM}) and solvation free (ΔG_{solv}) energies. The ΔE_{MM} term includes the internal (ΔE_{int}), electrostatic (ΔE_{ele}), and van der Waals (ΔE_{vdW}) energies, as shown in eq 3, while the ΔG_{solv} term is the sum of the electrostatic and nonpolar components as outlined by eq 4.

$$\Delta E_{MM} = \Delta E_{int} + \Delta E_{ele} + \Delta E_{vdW} \quad (3)$$

$$\Delta G_{solv} = \Delta G_{ele,solv} + \Delta G_{nonpolar,solv} \quad (4)$$

The $\Delta G_{ele,solv}$ was investigated by means of either the Poisson–Boltzmann (PB) or the generalized Born (GB) models, while $\Delta G_{nonpolar,solv}$ is calculated using solvent accessible surface area (SASA)^{43,44} with a probe radius of 1.4 Å using eq 5.

$$\Delta G_{nonpolar,solv} = \gamma SASA \quad (5)$$

Note that the dielectric constants were set to 1 and 80 for the solute and surrounding solvent, respectively. The value for surface tension constant γ of 0.0072 kcal/mol·Å² was used.

Decomposition Free Energy. The contribution of each residue toward the ligand binding was estimated using the per-residue decomposition free energy ($\Delta G_{bind}^{residue}$), based on the MM/GBSA approach. One half of the electrostatic interaction (E_{ele}^i) between atoms i and j of the protein and ligand, respectively, was taken to calculate the electrostatic contribution as outlined in eq 6.

$$E_{ele}^i = \frac{1}{2} \sum_{i \neq j} \frac{q_i q_j}{r_{ij}} \quad (6)$$

The q_i and q_j represent the atomic charges of atoms i and j , respectively, and r_{ij} is the distance between these two atoms. Alternatively, the per-residue intermolecular vdW interaction (E_{vdW}^i) was similarly attributed but avoiding double counting. The internal energy (ΔE_{int}) was equal to zero because of the internal energies of the complex, protein, and ligand that were calculated separately from the same trajectory. Therefore, the electrostatic free energy component based on the GB method was calculated by eq 7.

$$\Delta G_{ele,solv} = -\frac{1}{2} \left(1 - \frac{e^{-\kappa f_{GB}}}{\epsilon_\omega} \right) \sum_{ij} \frac{q_i q_j}{f_{GB}} \quad (7)$$

The dielectric constant of solvent (ϵ_ω) and the Debye–Hückel screening parameter (κ) were identified as 80 and 0, respectively, and f_{GB} is a smooth function interpolating between atomic radii and the distance between atoms i and j , in which the double sum runs over all pairs of atoms. Note that the common expression of f_{GB} was given by eq 8.

$$f_{GB} = \left[r_{ij}^2 + \alpha_i \alpha_j \exp\left(\frac{-r_{ij}^2}{4\alpha_i \alpha_j}\right) \right]^{1/2} \quad (8)$$

The α_i and α_j are the effective Born radii of atoms i and j , respectively. According to eqs 6 and 7, the contribution of atom i on the electrostatic free energy could be defined by eq 9.

$$\Delta G_{ele,solv}^i = -\frac{1}{2} \sum_{ij} \left(1 - \frac{e^{-k_f GB}}{\epsilon_\omega} \right) \frac{q_i q_j}{f_{GB}(r_{ij})} + \frac{1}{2} \sum_{i \neq j} \frac{q_i q_j}{r_{ij}} \quad (9)$$

In addition, the SASA of atom i in the complex and the separated parts in the nonpolar component was given by eq 10.

$$\Delta G_{nonpolar,solv}^i = \gamma \times (SASA^{i,com} - (SASA^{i,prot} + SASA^{i,lig})) \quad (10)$$

The $SASA^{i,prot}$ and $SASA^{i,lig}$ are equal to zero depending on which molecule the atom belonged to.

Taken altogether, the $\Delta G_{bind}^{residue}$ was the summation of E_{ele}^i , E_{vdW}^i , $\Delta G_{nonpolar,solv}^i$, and $\Delta G_{ele,solv}^i$. Similarly, the binding free energy contributions of the residue, backbone, and side chain were calculated separately from the related atoms.

RESULTS AND DISCUSSION

Stability of Global Structures. To determine the stability of the four MD systems from three independent MD simulations, the RMSDs of all atoms relative to those of the starting structure versus the simulation time was plotted (Figure 3). The RMSD values rapidly increased in the first 5 ns

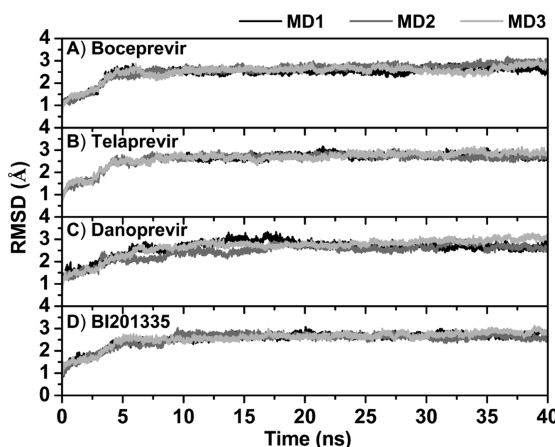


Figure 3. Root-mean square displacements (RMSDs) for all atoms of the four NS3/4A-inhibitor complexes compared to their initial structures from the three independent simulations (MD1–MD3).

and fluctuated at approximately 2.5 Å until 40 ns in all complexes. The NS3/4A–danoprevir complex showed a higher fluctuation level during 12–18 ns (about 2–3 Å) and subsequently reduced to 2.5 Å at 20 ns till the end of simulation. This is therefore the MD trajectories from 20 to 40 ns of the four studied systems were extracted for further analysis.

Key Residues for Ligand Binding. The per-residue decomposition of the binding free energy ($\Delta G_{bind}^{residue}$) based MM-GBSA approach was used to scan the key residues important for ligand binding to the HCV NS3/4A protease, with the contribution of protease residues in the four complexes being shown in Figure 4. Although the structures of the four inhibitors are significantly different (Figure 2), they share similar orientations and binding interactions at the protease active site (Figure 1B). From the fingerprint in Figure 4, NS3 residues 41–43, 57, 81, 132–139, 155–159, and 168 are likely to

have provided an energy stabilization of < -1 kcal/mol toward ligand binding, while there is no contribution from the NS4A cofactor (data not shown). The stabilization from these residues including the other residues within 8 Å sphere around ligand was separately considered into the contribution from their backbone and side chain in Figure 5 (left), as well as in terms of the electrostatic ($\Delta E_{ele} + \Delta G_{polar}$) and vdW ($\Delta E_{vdW} + \Delta G_{nonpolar}$) energies in Figure 5 (right). Among the 24 residues plotted in Figure 5 (left), most residues likely stabilized the ligand through the backbone, such as residues G137, S138, A157, V158, and D168. All the residues greatly contributed to ligand binding through the vdW energetic term (up to -4.5 kcal/mol) mainly at the residues H57, D81 (only for BI201335), R155, A156, A157, and V158 (only for telaprevir and BI201335) with interactions of < -2.0 kcal/mol (Figure 5, right). Meanwhile, their electrostatic energies were detected in the range of 2.4 to -2.0 kcal/mol in which the positive and negative values indicated the ligand destabilization and stabilization, accordingly. The obtained data resulted from the hydrophobic S3 and S4 subsites, the partially hydrophobic/hydrophilic S1 and S1' subsites, and the extended hydrophilic S2 subsite (Figure 1).²⁰

As mentioned above that the binding patterns of the four inhibitors were typically comparable, however, the interactions at the two side chains of covalent and noncovalent inhibitors were different (Figure 5 (left)). For noncovalent inhibitors, the fluoroisoindoline and bromoquinoline rings at the extended P2 site of danoprevir and BI201335 (Figure 2) were highly stabilized by the R155 residue especially by its aliphatic side chain through the vdW interaction. This strong hydrophobic contribution has been mostly found for protease inhibitors containing the aromatic ring at the extended P2 site^{13,22,23,45,46} associated with the highly resistance to several anti-HCV drugs.^{21,47–49} Meanwhile, the K136 residue strongly interacted with their P1'-sulfonyl and P1-carboxylate groups, respectively. More different interactions were observed as follows. The strongest stabilization from the NS3/4A protease was found for danoprevir binding (Figure 5, left), where the ten residues (F43, H57, K136, G137, S138, S139, R155, A156, A157, and V158) each provided an energetic contribution of < -1 kcal/mol. Of the three catalytic residues in the BI201335 complex, H57 provided the highest stabilization to the ligand (-4.6 kcal/mol in Figure 5, left), while the attractive contribution from the neutral D81 residue was only found in this system. In contrast, there was rather low stabilization from S139 which is the residue center for the cleavage reaction in accordance with the predicted weak H-bonds at 11% and 47% occupancy (Figure 6). Higher stabilization by residue D168 was found for BI201335 binding (-1.2 kcal/mol), and in addition the Y56, V78, and Q80 residues (-1.3 , -0.8 , and -0.8 kcal/mol, respectively) likely supported its extended P2 site. In addition, the salt bridge formation between R155 and D168 was only detected in danoprevir and BI201335 complexes (Figure 7); therefore, the R155 conformation can be eventually affected by D168 mutation possibly related to the macrocyclic drug resistances.⁷ This was formerly seen in the NS3/4A-TMC435 complex in which the energy change profile of TMC435 suggested the interrupted interaction at the extended P2 site.⁴⁶ Alternatively, the Q41 and T42 residues at the N-terminus attractively interacted with the α -ketoamide at the P1 site of boceprevir via electrostatic interactions of -0.5 and -1.1 kcal/mol, respectively (Figure 5, right) with a formation of three strong H-bonds (>70% occupation in Figure 6). Lastly, although the lowest energetic contribution was presented in the telaprevir complex, the C159 residue conferred a higher

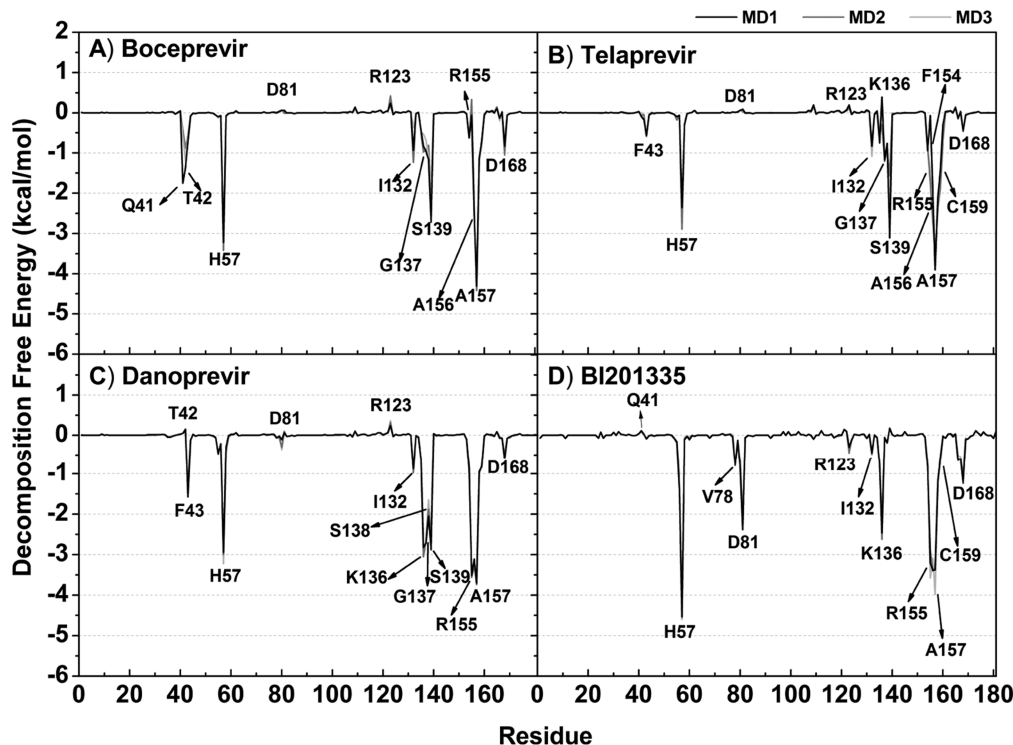


Figure 4. Per-residue decomposition free energy ($\Delta G_{bind}^{residue}$) of the NS3 protease for the four studied inhibitors from the three independent simulations.

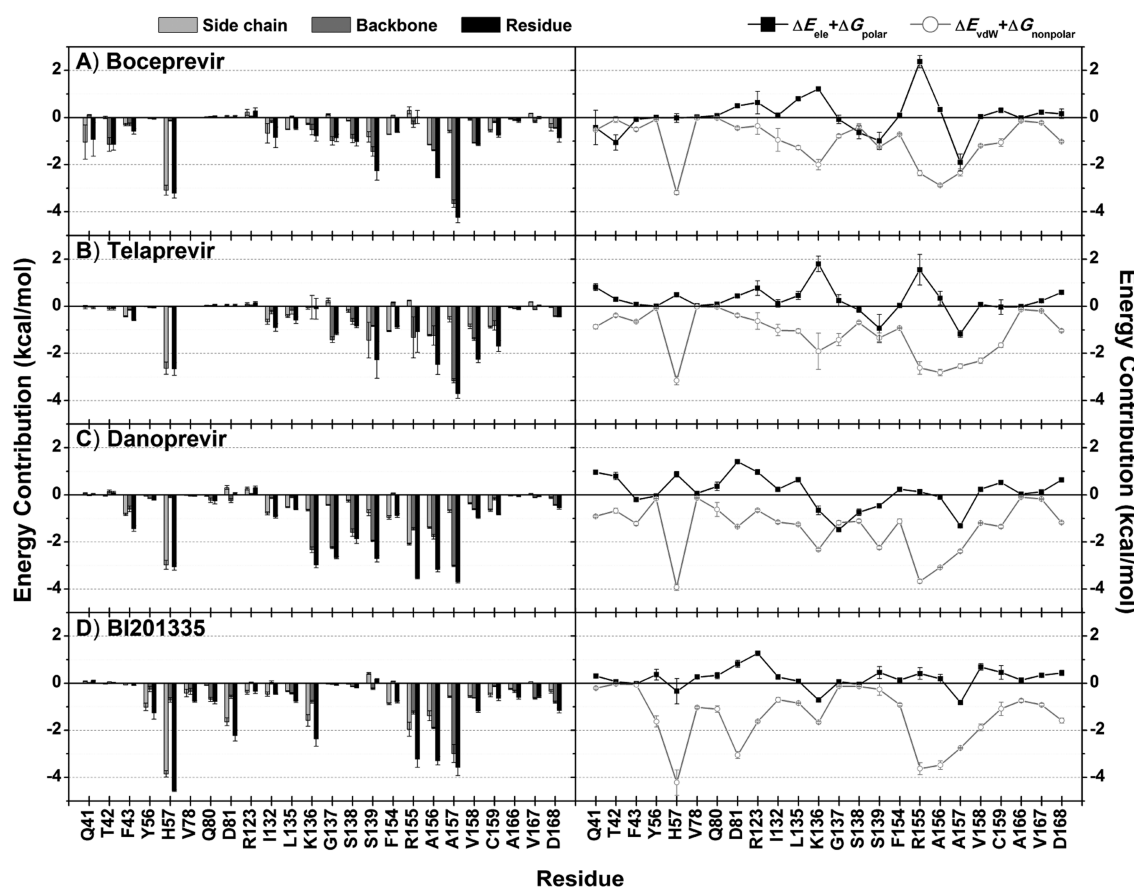


Figure 5. (Left) Averaged energy contributions over the three independent simulations from the residue backbone and side chain for the four studied complexes of the NS3/4A protease with (A) boceprevir, (B) telaprevir, (C) danoprevir, and (D) BI201335. (Right) Averaged electrostatic ($\Delta E_{ele}^* + \Delta G_{polar}^*$) and vdW ($\Delta E_{vdW}^* + \Delta G_{nonpolar}^*$) energy contributions from each residue. Note the standard deviation among the three simulations is shown as an error bar.

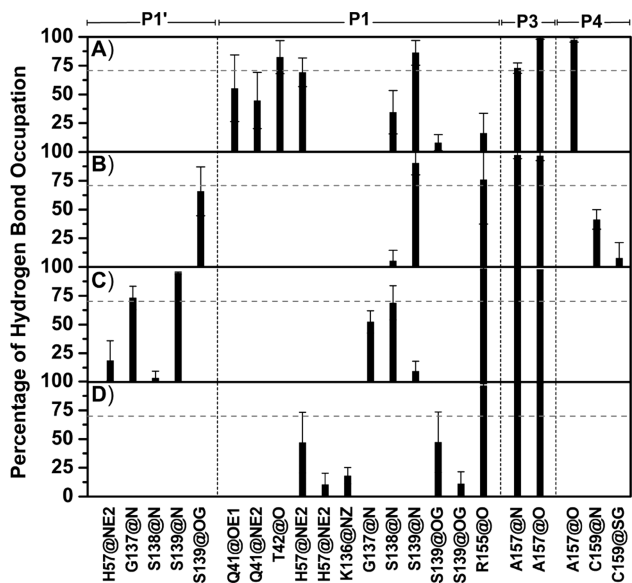


Figure 6. The averaged percentage of H-bond occupation of the NS3/4A residues contributed to (A) boceprevir, (B) telaprevir, (C) danoprevir, and (D) BI201335 over the three MD simulations where the standard deviation is given as an error bar.

stabilization in this system than the other three inhibitors by ~1 kcal/mol (Figure 5, left) mainly through vdW interaction (right).

Hydrogen Bond (H-Bond) Interactions. Even though ligand binding was predominantly contributed by the vdW interactions as mentioned above, H-bond formation between the ligand and the surrounding residues of NS3/4A could be an important factor in the specific inhibition toward this targeted enzyme. Therefore, H-bond interactions were evaluated in terms of the percentage of H-bond occupation using the criteria of (i) a distance between the proton donor and acceptor atoms $\leq 3.5 \text{ \AA}$ and (ii) the angle of the H-bond ≥ 120 degree. Boceprevir and BI201335 were comprised of P1–P4 sites, whereas the P1' site is additionally connected to the P1 site in the cases of telaprevir and danoprevir (see Figure 2). In order to reveal the specific binding at each subsite of NS3/4A, the H-bond interactions were separately considered for the individual P site of inhibitor as shown in Figure 6, and the 3D structure taken from the last MD snapshot of the MD1 simulation was chosen to display the inhibitor binding and interaction at the protease active site in Figure 7.

By considering the number of strong H-bonds (>70% occupancy) with the NS3 residue (Figure 6), the order of H-bond strength was of boceprevir (6) > danoprevir (5) > telaprevir (4) > BI201335 (3).

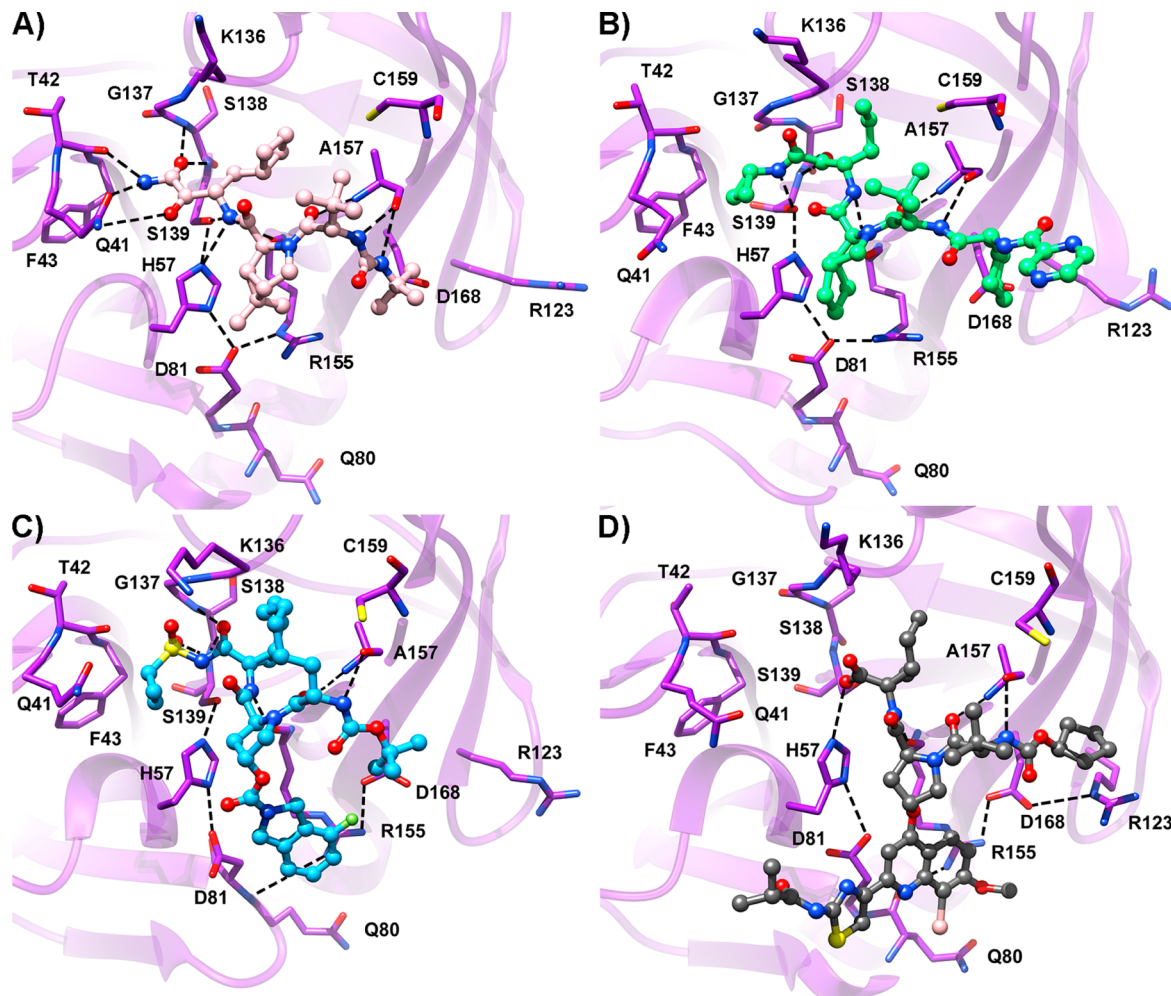


Figure 7. The binding pattern of (A) boceprevir, (B) telaprevir, (C) danoprevir, and (D) BI201335 in the NS3/4A active site demonstrated from the last snapshot from MD1 simulation. Note that residue H57 is in the HIE type and D81 is in neutral form for the NS3/4A-BI201335 complex, while in the other complexes they are the HID type and negatively charged form, respectively.

Table 1. Comparison of the Averaged Binding Free Energy and Energetic Components (kcal/mol) Calculated Using 100×3 MD Trajectories from the Three Independent Simulations and Experimental IC_{50} and K_i (nM) Values of the Four Inhibitors Binding to the NS3/4A Protease of HCV

| | Boceprevir | | Telaprevir | | Danoprevir | | BI201335 | |
|--|------------------|------------------|------------------|------------------|------------------|------------------|-------------------|------------------|
| | MM/PBSA | MM/GBSA | MM/PBSA | MM/GBSA | MM/PBSA | MM/GBSA | MM/PBSA | MM/GBSA |
| ΔE_{ele} | -39.8 ± 7.5 | | -44.3 ± 7.9 | | -69.2 ± 6.9 | | -194.9 ± 22.4 | |
| ΔE_{vdW} | -46.3 ± 3.2 | | -56.0 ± 3.6 | | -66.8 ± 2.9 | | -67.3 ± 4.0 | |
| ΔE_{MM} | -86.1 ± 7.9 | | -100.3 ± 8.8 | | -136.1 ± 7.2 | | -262.2 ± 21.8 | |
| $\Delta G_{nonpolar,sol}$ | -6.1 ± 0.3 | | -7.2 ± 0.4 | | -7.9 ± 0.3 | | 8.7 ± 0.3 | |
| $\Delta G_{ele,sol}$ | 48.7 ± 3.8 | 45.7 ± 4.1 | 60.9 ± 6.8 | 57.7 ± 6.8 | 86.9 ± 6.0 | 78.1 ± 5.2 | 213.3 ± 20.3 | 213.7 ± 20.5 |
| ΔG_{sol} | 42.6 ± 3.8 | 39.6 ± 4.0 | 53.7 ± 6.7 | 50.5 ± 6.7 | 79.1 ± 6.0 | 70.2 ± 5.1 | 204.7 ± 20.2 | 205.1 ± 20.4 |
| $\Delta G_{ele,sol} + \Delta E_{ele}$ | 8.9 ± 5.8 | 5.9 ± 5.8 | 16.6 ± 3.7 | 13.4 ± 3.2 | 17.7 ± 3.4 | 8.8 ± 3.3 | 18.4 ± 5.8 | 18.8 ± 3.8 |
| $\Delta G_{nonpolar,sol} + \Delta E_{vdW}$ | -52.4 ± 1.8 | | -63.2 ± 1.9 | | -74.7 ± 1.6 | | -75.9 ± 2.2 | |
| ΔG_{total} | -43.5 ± 6.1 | -46.5 ± 5.5 | -46.6 ± 4.4 | -49.8 ± 4.0 | -56.9 ± 3.9 | -65.8 ± 4.0 | -57.5 ± 5.1 | -57.2 ± 3.8 |
| $-T\Delta S$ | 27.2 ± 16.6 | | 33.1 ± 17.1 | | 29.4 ± 16.1 | | 33.8 ± 16.6 | |
| ΔG_{bind} | -16.3 ± 11.4 | -19.4 ± 11.1 | -13.5 ± 10.8 | -16.7 ± 10.6 | -27.5 ± 10.0 | -36.4 ± 10.0 | -23.7 ± 10.9 | -23.4 ± 10.2 |
| IC_{50} (nM) | 80 ± 15 | | 87 ± 5 | | 0.20 ± 0.01 | | — | |
| K_i (nM) | 1.1 ± 0.3 | | 3.2 ± 1.1 | | — | | 1.2 ± 0.2 | |

All four inhibitors had no H-bond formation at the S2 subsite, although the two noncovalent inhibitors, danoprevir and BI201335, consisted of the fluoroisoindoline and bromoquino-line rings (Figure 2). Only two strong H-bonds with the backbone of A157 toward the P3 site at the carbamate nitrogen of danoprevir and BI201335 as well as the amide group of boceprevir and telaprevir were maintained as in their initial cocrystal structures.^{19,20} This might imply that the A157 backbone of the NS3 protease is a recognized site for ligand binding. They also shared the same interaction with R155 at the amide nitrogen of the P1 cleavage site but with different binding strengths. Note that these results were in accordance with the previous theoretical and experimental studies.^{13,45} Therefore the H-bond with R155 could be a common interaction between NS3/4A and inhibitors. In comparison with a potent macrocyclic inhibitor TMC435,⁴⁶ the H-bond formed between the backbone of A157 and the P3 nitrogen of TMC435 was absent because this nitrogen atom was capped by the methyl group. More than 75% H-bond occupation with R155 was detected for danoprevir, BI201335 and telaprevir, whereas the interaction was rather weak for boceprevir (<17%) with increased H-bond distance by ~0.8 Å at the end of the MD simulations (Figure 7A). Moreover, the P1-ketoamide of boceprevir in planar orientation (Figure 7A) was well formed the five hydrogen bonds with Q41, T42, H57, and S139, while the interaction with S139 was only maintained in telaprevir due to the cyclopropyl termination at the P1' site (Figures 6 and 7). The latter one is somewhat similar to that found for danoprevir, which contains a cyclopropylsulfonyl group, but the amide oxygen at the P1 site was stabilized by S138 instead. Differentially, the carboxylate group at the P1 site of BI201335 formed five weak H-bonds with H57, K136, and S139 (Figure 6D). At the P4 site (Figures 2 and 6), the peptide nitrogen of boceprevir strongly interacted with the A157 backbone oxygen, while this interaction could not be formed with danoprevir and BI201335 because of the change of this nitrogen to the carbamate oxygen. Instead, a 41% and an 8% H-bond occupation were detected between C159 and the P4-amino oxygen of telaprevir. The P1' site of telaprevir and danoprevir made a strong H-bond with the side chain and backbone of S139, respectively. Additionally, that of danoprevir also formed a strong H-bond with a side chain of G137.

Binding Affinity Predictions. Both MM/PBSA and MM/GBSA methods were employed in this study to estimate and

compare the inhibitory efficiency of the four studied inhibitors against the HCV NS3/4A protease in terms of the binding free energy (ΔG_{bind}) and its energetic components (gas phase energy (ΔE_{MM}), which is comprised of ΔE_{vdW} and ΔE_{ele} energies, solvation free energy (ΔG_{sol}), and the entropic term ($-T\Delta S$)), as summarized in Table 1. It seems that the total negative charge ($-1e$) of BI201335 favorably enhanced electrostatic energy interaction toward the NS3/4A protease (ΔE_{ele} of -194.9 kcal/mol) by ~three- to five-fold relative to the other three inhibitors (-69.2 , -44.3 , and -39.8 kcal/mol for danoprevir, telaprevir, and boceprevir, respectively). The ΔE_{vdW} and ΔE_{ele} almost equally contributed to the danoprevir binding, while the higher stabilization by ΔE_{vdW} of 6 and 12 kcal/mol was found for boceprevir and telaprevir. Although the ΔE_{ele} contribution was relatively high in the BI201335 complex, the ΔE_{vdW} contribution in this complex (-67.3 kcal/mol) was in the same range to that of the danaprevir complex (-66.8 kcal/mol). By including the solvation free energy, the vdW term ($\Delta G_{nonpolar,sol} + \Delta E_{vdW}$) is a favorable contribution to the total binding free energies of all four NS3/4A inhibitor complexes, which were opposed by the unfavorable electrostatic term ($\Delta G_{ele,sol} + \Delta E_{ele}$). This is due to relatively high positive values of polar solvation resulting from either PB or GB models. So, the vdW interaction played an important role in the HCV NS3/4A protease with inhibitors in good agreement with our previous study.⁵⁰ With a summation of the entropic term, both MM/PBSA and MM/GBSA methods agreed with each other in binding free energy prediction of danoprevir (-27.5 and -36.4 kcal/mol) > BI201335 (-23.7 and -23.4 kcal/mol) > boceprevir (-16.3 and -19.4 kcal/mol) > telaprevir (-13.5 and -16.7 kcal/mol). The obtained results were relatively consistent with the experimental IC_{50} value⁸ rather than the K_i value.^{8,9}

CONCLUSION

In this work, the multiple 40-ns classical MD simulations were applied to the HCV NS3/4A protease in complex with the two existing anti-HCV drugs, boceprevir and telaprevir, and the two highly potent inhibitors, danoprevir and BI201335, currently in the clinical trial phase 2 and phase 3, respectively. Scanning of the per-residue decomposition free energy from the NS3 and NS4A domains revealed that the ligand binding was favorably stabilized by the NS3 residues 41–43, 57, 81, 132–139, 155–159, and 168 without any contribution from the NS4A domain.

In addition to the free energy contributed from the individual residues, the total MM/PBSA and MM/GBSA binding free energies also likely suggested that the vdW energetic term is the key ligand-target interaction for the NS3/4A protease of HCV. This is possibly because the binding site contains the hydrophobic residues at the extended S2, S3, and S4 subsites as well as partly at the S1' and S1 subsites. Besides the importance of vdW interaction, the intermolecular H-bonds were highly formed at the reactive P1 site of all inhibitors (the cleavage reaction center), while their P3 site sustainably interacted with the A157 backbone. Taken altogether, the ligand-target interactions and total binding free energies revealed that the order of the studied inhibitor susceptibilities was of danoprevir > BI201335 > boceprevir > telaprevir, which was in a somewhat similar trend to the experimentally derived data.

AUTHOR INFORMATION

Corresponding Author

*Phone: +6622185426. Fax: +6622185418. E-mail: t.rungtromongkol@gmail.com.

Notes

The authors declare no competing financial interest.

ACKNOWLEDGMENTS

This work was supported by the Higher Education Research Promotion and National Research University Project of Thailand, Office of the Higher Education Commission and the Thai Government Stimulus Package 2 (TKK2555) under the Project for Establishment of Comprehensive Center for Innovative Food, Health Products, and Agriculture. A.M. thanks the Royal Golden Jubilee Ph.D. Program (PHD/0271/2549), and T.R. is thankful for the grants for the development of new faculty staff (the Ratchadapiseksomphot Endowment Fund).

ABBREVIATIONS

HCV, hepatitis C virus; MM, molecular mechanic; PBSA, Poisson–Boltzmann surface area; GBSA, generalized Born surface area; PEG-IFN, peg-interferon; MD, molecular dynamics; (ss)RNA, single-stranded ribonucleic acid; PDB, Protein Data Bank; ^1H NMR, proton nuclear magnetic resonance spectroscopy; AMBER, assisted model building with energy refinement; HF, Haetree-Fock; ESP, electrostatic potential; RESP, restrained electrostatic potential; GAFF, general AMBER force field; SD, steepest descent; CG, conjugated gradient; PME, particle mesh Ewald; RMSD, root-mean-square displacement; H-bond, hydrogen bond; vdW, van der Waals; SASA, solvent accessible surface area

REFERENCES

- Lauer, G. M.; Walker, B. D. Hepatitis C Virus Infection. *N. Engl. J. Med.* **2001**, *345*, 41–52.
- Bostan, N.; Mahmood, T. An Overview about Hepatitis C: A Devastating Virus. *Crit. Rev. Microbiol.* **2010**, *36*, 91–133.
- Durantel, D.; Escuret, V.; Zoulim, F. Current and Emerging Therapeutic Approaches to Hepatitis C Infection. *Expert. Rev. Anti-Infect. Ther.* **2003**, *1*, 441–454.
- Ferguson, M. C. Current Therapies for Chronic Hepatitis C. *Pharmacotherapy* **2010**, *31*, 92–111.
- Fried, M. W.; Shiffman, M. L.; Reddy, K. R.; Smith, C.; Marinos, G.; Goncales, F. L., Jr.; Haussinger, D.; Diago, M.; Carosi, G.; Dhumeaux, D.; Craxi, A.; Lin, A.; Hoffman, J.; Yu, J. Peginterferon Alfa-2a Plus Ribavirin for Chronic Hepatitis C Virus Infection. *N. Engl. J. Med.* **2002**, *347*, 975–982.
- Yi, M.; Villanueva, R. A.; Thomas, D. L.; Wakita, T.; Lemon, S. M. Production of Infectious Genotype 1a Hepatitis C Virus (Hutchinson Strain) in Cultured Human Hepatoma Cells. *Proc. Natl. Acad. Sci. U. S. A.* **2006**, *103*, 2310–2315.
- Lagace, L.; White, P. W.; Bousquet, C.; Dansereau, N.; Do, F.; Llinas-Brunet, M.; Marquis, M.; Massariol, M. J.; Maurice, R.; Spickler, C.; Thibeault, D.; Triki, I.; Zhao, S.; Kukolj, G. In Vitro Resistance Profile of the Hepatitis C Virus NS3 Protease Inhibitor BI 201335. *Antimicrob. Agents Chemother.* **2012**, *56*, 569–572.
- Seiwert, S. D.; Andrews, S. W.; Jiang, Y.; Serebryany, V.; Tan, H.; Kossen, K.; Rajagopalan, P. T.; Misialek, S.; Stevens, S. K.; Stoycheva, A.; Hong, J.; Lim, S. R.; Qin, X.; Rieger, R.; Condroski, K. R.; Zhang, H.; Do, M. G.; Lemieux, C.; Hingorani, G. P.; Hartley, D. P.; Josey, J. A.; Pan, L.; Beigelman, L.; Blatt, L. M. Preclinical Characteristics of the Hepatitis C Virus NS3/4A Protease Inhibitor ITMN-191 (R7227). *Antimicrob. Agents Chemother.* **2008**, *52*, 4432–4441.
- White, P. W.; Llinas-Brunet, M.; Amad, M.; Bethell, R. C.; Bolger, G.; Cordingley, M. G.; Duan, J.; Garneau, M.; Lagace, L.; Thibeault, D.; Kukolj, G. Preclinical Characterization of BI 201335, a C-terminal Carboxylic Acid Inhibitor of the Hepatitis C Virus NS3-NS4A Protease. *Antimicrob. Agents Chemother.* **2010**, *54*, 4611–4618.
- (10) da Cunha, E. F. F.; Ramalho, T. C.; Taft, C. A.; de Alencastro, R. B. Computer-Assisted Analysis of the Interactions of Macrocyclic Inhibitors with Wild Type and Mutant D168A Hepatitis C Virus NS3 Serine Protease. *Lett. Drug Des. Discovery* **2006**, *3*, 17–28.
- Ontoria, J. M.; Di Marco, S.; Conte, I.; Di Francesco, M. E.; Gardelli, C.; Koch, U.; Matassa, V. G.; Poma, M.; Steinkühler, C.; Volpari, C.; Harper, S. The Design and Enzyme-bound Crystal Structure of Indoline Based Peptidomimetic Inhibitors of Hepatitis C Virus NS3 Protease. *J. Med. Chem.* **2004**, *47*, 6443–6446.
- Wei, H. Y.; Lu, C. S.; Lin, T. H. Exploring the P2 and P3 Ligand Binding Features for Hepatitis C Virus NS3 Protease Using Some 3D QSAR Techniques. *J. Mol. Graphics Modell.* **2008**, *26*, 1131–1144.
- Xue, W.; Wang, M.; Jin, X.; Liu, H.; Yao, X. Understanding the Structural and Energetic Basis of Inhibitor and Substrate Bound to the Full-Length NS3/4A: Insights from Molecular Dynamics Simulation, Binding Free Energy Calculation and Network Analysis. *Mol. Biosyst.* **2012**, *8*, 2753–2765.
- Lin, C. HCV NS3–4A Serine Protease. In *Hepatitis C viruses: Genomes and molecular biology*; Tan, S. L., Ed.; Horizon Bioscience: Norfolk, 2006; Chapter 6, pp 163–206.
- Lin, K. Development of Novel Antiviral Therapies for Hepatitis C Virus. *Virol. Sin.* **2010**, *25*, 246–266.
- Lindenbach, B. D.; Rice, C. M. Unravelling Hepatitis C Virus Replication from Genome to Function. *Nature* **2005**, *436*, 933–938.
- Love, R. A.; Parge, H. E.; Wickersham, J. A.; Hostomsky, Z.; Habuka, N.; Moomaw, E. W.; Adachi, T.; Hostomska, Z. The Crystal Structure of Hepatitis C Virus NS3 Proteinase Reveals a Trypsin-like Fold and a Structural Zinc Binding Site. *Cell* **1996**, *87*, 331–342.
- Lemke, C. T.; Goudreau, N.; Zhao, S.; Hucke, O.; Thibeault, D.; Llinas-Brunet, M.; White, P. W. Combined X-ray, NMR, and Kinetic Analyses Reveal Uncommon Binding Characteristics of the Hepatitis C Virus NS3-NS4A Protease Inhibitor BI 201335. *J. Biol. Chem.* **2011**, *286*, 11434–11443.
- Perni, R. B.; Chandorkar, G.; Cottrell, K. M.; Gates, C. A.; Lin, C.; Lin, K.; Luong, Y.-P.; Maxwell, J. P.; Murcko, M. A.; Pitlik, J.; Rao, G.; Schairer, W. C.; Drie, J. V.; Wei, Y. Inhibitors of Hepatitis C Virus NS3-4A Protease. Effect of P4 Capping Groups on Inhibitory Potency and Pharmacokinetics. *Bioorg. Med. Chem. Lett.* **2007**, *17*, 3406–3411.
- Prongay, A. J.; Guo, Z.; Yao, N.; Pichardo, J.; Fischmann, T.; Strickland, C.; Myers, J.; Weber, P. C.; Beyer, B. M.; Ingram, R.; Hong, Z.; Prosise, W. W.; Ramanathan, L.; Taremi, S. S.; Yarosh-Tomaine, T.; Zhang, R.; Senior, M.; Yang, R.-S.; Malcolm, B.; Arasappan, A.; Bennett, F.; Bogen, S. L.; Chen, K.; Jao, E.; Liu, Y.-T.; Lovey, R. G.; Saksena, A. K.; Venkatraman, S.; Girijavallabhan, V.; Njoroge, F. G.; Madison, V. Discovery of the HCV NS3/4A Protease Inhibitor (1R,SS)-N-[3-Amino-1-(cyclobutylmethyl)-2,3-dioxopropyl]-3-[2(S)-

- [[[(1,1-dimethylethyl)amino]carbonyl]amino]-3,3-dimethyl-1-oxobutyl]-6,6-dimethyl-3-azabicyclo[3.1.0]hexan-2(S)-carboxamide (Sch 503034) II. Key Steps in Structure-Based Optimization. *J. Med. Chem.* **2007**, *50*, 2310–2318.
- (21) Romano, K. P.; Ali, A.; Royer, W. E.; Schiffer, C. A. Drug Resistance Against HCV NS3/4A Inhibitors Is Defined by the Balance of Substrate Recognition versus Inhibitor Binding. *Proc. Natl. Acad. Sci.* **2010**, *107*, 20986–20991.
- (22) Xue, W.; Ban, Y.; Liu, H.; Yao, X. Computational Study on the Drug Resistance Mechanism against HCV NS3/4A Protease Inhibitors Vaniprevir and MK-5172 by the Combination Use of Molecular Dynamics Simulation, Residue Interaction Network, and Substrate Envelope Analysis. *J. Chem. Inf. Model.* **2014**, *54*, 621–633.
- (23) Romano, K. P.; Ali, A.; Aydin, C.; Soumana, D.; Özen, A.; Deveau, L. M.; Silver, C.; Cao, H.; Newton, A.; Petropoulos, C. J.; Huang, W.; Schiffer, C. A. The Molecular Basis of Drug Resistance against Hepatitis C Virus NS3/4A Protease Inhibitors. *PLoS Pathog.* **2012**, *8*, e1002832.
- (24) Tong, L.; Wengler, G.; Rossmann, M. G. Refined Structure of Sindbis Virus Core Protein and Comparison with Other Chymotrypsin-like Serine Proteinase Structures. *J. Mol. Biol.* **1993**, *230*, 228–247.
- (25) De Francesco, R.; Steinkuhler, C. Structure and Function of the Hepatitis C Virus NS3-NS4A Serine Proteinase. *Curr. Top. Microbiol. Immunol.* **2000**, *242*, 149–169.
- (26) Frecer, V.; Kabelac, M.; De Nardi, P.; Prich, S.; Miertus, S. Structure-Based Design of Inhibitors of NS3 Serine Protease of Hepatitis C Virus. *J. Mol. Graphics Modell.* **2004**, *22*, 209–220.
- (27) Gallinari, P.; Brennan, D.; Nardi, C.; Brunetti, M.; Tomei, L.; Steinkühler, C.; De Francesco, R. Multiple Enzymatic Activities Associated with Recombinant NS3 Protein of Hepatitis C Virus. *J. Virol.* **1998**, *72*, 6758–6769.
- (28) Johansson, A.; Hubatsch, I.; Akerblom, E.; Lindeberg, G.; Winiwarter, S.; Danielson, U. H.; Hallberg, A. Inhibition of Hepatitis C Virus NS3 Protease Activity by Product-Based Peptides is Dependent on Helicase Domain. *Bioorg. Med. Chem. Lett.* **2001**, *11*, 203–206.
- (29) Case, D. A.; Cheatham, T. E.; Darden, T.; Gohlke, H.; Luo, R.; Merz, K. M.; Onufriev, A.; Simmerling, C.; Wang, B.; Woods, R. J. The Amber Biomolecular Simulation Programs. *J. Comput. Chem.* **2005**, *26*, 1668–1688.
- (30) Olsson, M. H. M.; Søndergaard, C. R.; Rostkowski, M.; Jensen, J. H. PROPKA3: Consistent Treatment of Internal and Surface Residues in Empirical pKa Predictions. *J. Chem. Theory Comput.* **2011**, *7*, 525–537.
- (31) Duan, Y.; Wu, C.; Chowdhury, S.; Lee, M. C.; Xiong, G.; Zhang, W.; Yang, R.; Cieplak, P.; Luo, R.; Lee, T.; Caldwell, J.; Wang, J.; Kollman, P. A Point-Charge Force Field for Molecular Mechanics Simulations of Proteins Based on Condensed-Phase Quantum Mechanical Calculations. *J. Comput. Chem.* **2003**, *24*, 1999–2012.
- (32) Frisch, M. J.; Trucks, G. W.; Schlegel, H. B.; Scuseria, G. E.; Robb, M. A.; Cheeseman, J. R.; Montgomery, J. A., Jr.; Vreven, T.; Kudin, K. N.; Burant, J. C.; Millam, J. M.; Iyengar, S. S.; Tomasi, J.; Barone, V.; Mennucci, B.; Cossi, M.; Scalmani, G.; Rega, N.; Petersson, G. A.; Nakatsuji, H.; Hada, M.; Ehara, M.; Toyota, K.; Fukuda, R.; Hasegawa, J.; Ishida, M.; Nakajima, T.; Honda, Y.; Kitao, O.; Nakai, H.; Klene, M.; Li, X.; Knox, J. E.; Hratchian, H. P.; Cross, J. B.; Bakken, V.; Adamo, C.; Jaramillo, J.; Gomperts, R.; Stratmann, R. E.; Yazayev, O.; Austin, A. J.; Cammi, R.; Pomelli, C.; Ochterski, J. W.; Ayala, P. Y.; Morokuma, K.; Voth, G. A.; Salvador, P.; Dannenberg, J. J.; Zakrzewski, V. G.; Dapprich, S.; Daniels, A. D.; Strain, M. C.; Farkas, O.; Malick, D. K.; Rabuck, A. D.; Raghavachari, K.; Foresman, J. B.; Ortiz, J. V.; Cui, Q.; Baboul, A. G.; Clifford, S.; Cioslowski, J.; Stefanov, B. B.; Liu, G.; Liashenko, A.; Piskorz, P.; Komaromi, I.; Martin, R. L.; Fox, D. J.; Keith, T.; Al-Laham, M. A.; Peng, C. Y.; Nanayakkara, A.; Challacombe, M.; Gill, P. M. W.; Johnson, B.; Chen, W.; Wong, M. W.; Gonzalez, C.; Pople, J. A. Gaussian 03, Revision C.02; Gaussian, Inc.: Wallingford, CT, 2004.
- (33) Wang, J.; Wolf, R. M.; Caldwell, J. W.; Kollman, P. A.; Case, D. A. Development and Testing of a General Amber Force Field. *J. Comput. Chem.* **2004**, *25*, 1157–1174.
- (34) Jorgensen, W. L.; Chandrasekhar, J.; Madura, J. D.; Impey, R. W.; Klein, M. L. Comparison of Simple Potential Functions for Simulating Liquid Water. *J. Chem. Phys.* **1983**, *79*, 926–935.
- (35) Ryckaert, J.-P.; Cicotti, G.; Berendsen, H. J. C. Numerical Integration of the Cartesian Equations of Motion of a System with Constraints: Molecular Dynamics of n-Alkanes. *J. Comput. Phys.* **1977**, *23*, 327–341.
- (36) York, D. M.; Darden, T. A.; Pedersen, L. G. The Effect of Long-Range Electrostatic Interactions in Simulations of Macromolecular Crystals - a Comparison of the Ewald and Truncated List Methods. *J. Chem. Phys.* **1993**, *99*, 8345–8348.
- (37) Hou, T.; Wang, J.; Li, Y.; Wang, W. Assessing the Performance of the MM/PBSA and MM/GBSA Methods. 1. The Accuracy of Binding Free Energy Calculations Based on Molecular Dynamics Simulations. *J. Chem. Inf. Model.* **2011**, *51*, 69–82.
- (38) Li, X.; Zhang, W.; Qiao, X.; Xu, X. Prediction of Binding for a Kind of Non-Peptic HCV NS3 Serine Protease Inhibitors from Plants by Molecular Docking and MM/PBSA Method. *Bioorg. Med. Chem.* **2007**, *15*, 220–226.
- (39) Kaiyawet, N.; Rungrotmongkol, T.; Hannongbua, S. Effect of Halogen Substitutions on dUMP to Stability of Thymidylate Synthase/dUMP/mTHF Ternary Complex Using Molecular Dynamics Simulation. *J. Chem. Inf. Model.* **2013**, *53*, 1315–1323.
- (40) Khuntawee, W.; Rungrotmongkol, T.; Hannongbua, S. Molecular Dynamic Behavior and Binding Affinity of Flavonoid Analogue to the Cyclin Dependent Kinase 6/Cyclin D Complex. *J. Chem. Inf. Model.* **2012**, *52*, 76–83.
- (41) Meeprasert, A.; Khuntawee, W.; Kamlungsua, K.; Nunthaboot, N.; Rungrotmongkol, T.; Hannongbua, S. Binding Pattern of the Long Acting Neuraminidase Inhibitor Laninamivir towards Influenza A Subtypes H5N1 and Pandemic H1N1. *J. Mol. Graphics Modell.* **2012**, *38*, 148–154.
- (42) Rungrotmongkol, T.; Nunthaboot, N.; Malaisree, M.; Kaiyawet, N.; Yotmanee, P.; Meeprasert, A.; Hannongbua, S. Molecular Insight into the Specific Binding of ADP-Ribose to the nsP3Macro Domains of Chikungunya and Venezuelan Equine Encephalitis Viruses: Molecular Dynamics Simulations and Free Energy Calculations. *J. Mol. Graphics Modell.* **2010**, *29*, 347–353.
- (43) Gohlke, H.; Case, D. A. Converging Free Energy Estimates: MM-PB(GB)SA Studies on the Protein-Protein Complex Ras-Raf. *J. Comput. Chem.* **2004**, *25*, 238–250.
- (44) Kollman, P. A.; Massova, I.; Reyes, C.; Kuhn, B.; Huo, S.; Chong, L.; Lee, M.; Lee, T.; Duan, Y.; Wang, W.; Donini, O.; Cieplak, P.; Srinivasan, J.; Case, D. A.; Cheatham, T. E. Calculating Structures and Free Energies of Complex Molecules: Combining Molecular Mechanics and Continuum Models. *Acc. Chem. Res.* **2000**, *33*, 889–897.
- (45) Li, X.; Zhang, Y. K.; Liu, Y.; Ding, C. Z.; Zhou, Y.; Li, Q.; Plattner, J. J.; Baker, S. J.; Zhang, S.; Kazmierski, W. M.; Wright, L. L.; Smith, G. K.; Grimes, R. M.; Crosby, R. M.; Creech, K. L.; Carballo, L. H.; Slater, M. J.; Jarvest, R. L.; Thommes, P.; Hubbard, J. A.; Convery, M. A.; Nassau, P. M.; McDowell, W.; Skarzynski, T. J.; Qian, X.; Fan, D.; Liao, L.; Ni, Z. J.; Pennicott, L. E.; Zou, W.; Wright, J. Novel Macroyclic HCV NS3 Protease Inhibitors Derived from Alpha-Amino Cyclic Boronates. *Bioorg. Med. Chem. Lett.* **2010**, *20*, 5695–5700.
- (46) Xue, W.; Pan, D.; Yang, Y.; Liu, H.; Yao, X. Molecular Modeling Study on the Resistance Mechanism of HCV NS3/4A Serine Protease Mutants R155K, A156V and D168A to TMC435. *Antiviral Res.* **2012**, *93*, 126–137.
- (47) Halfon, P.; Locarnini, S. Hepatitis C Virus Resistance to Protease Inhibitors. *J. Hepatol.* **2011**, *55*, 192–206.
- (48) He, Y.; King, M. S.; Kempf, D. J.; Lu, L.; Lim, H. B.; Krishnan, P.; Kati, W.; Middleton, T.; Molla, A. Relative Replication Capacity and Selective Advantage Profiles of Protease Inhibitor-Resistant Hepatitis C Virus (HCV) NS3 Protease Mutants in the HCV

Genotype 1b Replicon System. *Antimicrob. Agents Chemother.* **2008**, *52*, 1101–1110.

(49) Lenz, O.; Verbinnen, T.; Lin, T.-I.; Vijgen, L.; Cummings, M. D.; Lindberg, J.; Berke, J. M.; Dehertogh, P.; Fransen, E.; Scholliers, A.; Vermeiren, K.; Ivens, T.; Raboisson, P.; Edlund, M.; Storm, S.; Vrang, L.; de Kock, H.; Fanning, G. C.; Simmen, K. A. In Vitro Resistance Profile of the Hepatitis C Virus NS3/4A Protease Inhibitor TMC435. *Antimicrob. Agents Chemother.* **2010**, *54*, 1878–1887.

(50) Meeprasert, A.; Rungrotmongkol, T.; Li, M. S.; Hannongbua, S. In Silico Screening for Potent Inhibitors against the NS3/4A Protease of Hepatitis C Virus. *Curr. Pharm. Des.* **2014**, DOI: 10.2174/13816128113199990632.